South African Journal of Chemical Engineering 26 (2018) 35–41

Contents lists available at ScienceDirect

South African Journal of Chemical Engineering

journal homepage: www.elsevier.com/locate/sajce

Corrosion inhibition properties of the combined admixture of essential oil extracts on mild steel in the presence of SO_4^{2-} anions

Roland Tolulope Loto*, Oluwatobilola Olowoyo

Department of Mechanical Engineering, Covenant University, Ota, Ogun State, Nigeria

ARTICLE INFO

Keywords:
Corrosion
Mild steel
Inhibition
Adsorption

ABSTRACT

The combined admixture of essential oil extracts, salvia officinalis and simmondsia chinensis was studied at low concentrations to assess their corrosion inhibition performance on mild steel in 1 M H_2SO_4 solution. Electrochemical studies were performed with potentiodynamic polarization test and weight loss analysis while open circuit potential measurement was employed to assess the thermodynamic stability of the corrosion properties of the compound with respect to time. Results obtained showed optimal inhibition efficiency of 86.58% and 83.29% at 6% and 5% volumetric concentration from the electrochemical test. The corrosion potential of the inhibited steel displaced significantly in the positive direction compared to the significant negative displacement of corroded steel due to surface coverage from the inhibitor molecules on the inhibited steel. Thermodynamic calculations showed chemisorption adsorption mechanism according to Langmuir, Frumkin and Freundlich adsorption isotherm models. Optical images of inhibited mild steel surface significantly contrast the corroded non-inhibited steel which showed the presence of surface oxides, general deterioration and macro pits.

1. Introduction

The problem of corrosion is prevalent in most industries and it account for a huge portion of revenue spent on maintenance due to corrosion damage (Corrosion Costs and Preve, 2018; Akinyemi et al., 2012; Jekayinfa et al., 2015). In numerous cases corrosion damage has resulted in attendant environmental problems due to leakage of degraded metallic components, plant shut down and collapse of structures (The effects and economic, 2000; K. Elaya, 2014). One of the major factors that influence the extent of corrosion failures is choice of materials for equipment, components and structures. Carbon steels are the most widely used steel due to its relatively low cost compared to the costly corrosion-resistant stainless steels. It is readily available and provides desirable material properties such as strength, weldability, ductility and hardness that make it the attractive choice for most engineering applications (Deepak et al., 2017). Due to the absence of some alloying elements such as Cr, Mo, Ni etc. carbon steel have very weak or no resistance to corrosion prevalent in industrial environment. As a result they deteriorate rapidly in the presence of corrosive species (SO_4^{2-}, Cl^- etc.). The most cost-effective means of prolonging the lifespan of industrial parts constructed from mild steel is the use of chemical compounds known as corrosion inhibitors (Camila and Alexandre, 2013). The most commonly applied corrosion inhibitors are chemicals of organic origin which act by forming a passive protective film on the steel surface (Kuznetsov, 1996; Sanyal, 1981; Fouda et al., 2017; Rivera-Grau et al., 2013; David, 2017). Most corrosion inhibitors are toxic and environmentally destructive hence the need for cost effect and sustainable replacements (Loto et al., 2013; Singh and Bockris, 1996; Winkler et al., 2014; CicekChromates, 2017). Chemical compounds from plant extract have been proven in previous research to be very promising for effect inhibition of metallic corrosion (Dakeshwar and Fahmida, 2015; Subhashini et al., 2010; Obot et al., 2010; Loto et al., 2018; Loto, 2017a; Essential oil). Essential oils are concentrated hydrophobic liquid consisting of volatile aroma compounds from plants. They are the oil of plants from which they were extracted by distillation, expression, solvent extraction, absolute oil extraction etc. Essential oils have extensive health benefits and are being explored for the treatment of a variety of diseases. This research aims to study the corrosion inhibition performance of salvia officinalis and simmondsia chinensis in dilute H_2SO_4 solution.

2. Experimental methods

Mild steel samples (MS) with a nominal wt. % composition shown in composition of the test specimen (Table 1) was obtained commercially from the open market and analyzed at the Materials characterization

* Corresponding author.
E-mail address: tolu.loto@gmail.com (R.T. Loto).

https://doi.org/10.1016/j.sajce.2018.09.002
Received 9 June 2018; Received in revised form 24 July 2018; Accepted 7 September 2018

Table 1
Percentage nominal composition of MS.

Element Symbol	Mn	P	S	C	Fe
% Composition (MS)	0.8	0.04	0.05	0.16	98.95

Laboratory, Department of Mechanical Engineering, Covenant University. The steel samples with cylindrical shape were machined to average dimensions with length of 1.1 cm and diameter of 1.15 cm. Metallographic preparation of the samples were performed with silicon carbide abrasive papers with grits of 120, 220, 320, 600, 800 and 1000. They were subsequently polished to 6um for corrosion tests. Salvia officinalis and simmondsia chinensis essential oils obtained from NOW Foods, USA with a combined molar mass of 2210.53 g/cm^3 are the organic compounds evaluated for their symbiotic corrosion inhibiting characteristics. The compounds (SASC) were prepared in the acid solution with combined molar concentrations of 4.52×10^3, 9.05×10^3, 1.36×10^2, 1.81×10^2, 2.26×10^2 and 2.71×10^2 in 400 mL of 1 H_2SO_4 acid solutions.

Polarization test was performed at 30 °C ambient temperature with a three electrode system with a transparent cell containing 200 mL of the H_2SO_4/SASC solution at specific SASC concentrations with Digi-Ivy 2311 electrochemical workstation. MS embedded in acrylic resin with exposed surface area of 1.13 cm^2 was the working electrode while platinum rod was used as the counter electrode and silver chloride electrode (Ag/AgCl) as the reference electrode. Potentiodynamic polarization plots were obtained at a scan rate of 0.0015 V/s between potentials of −0.7 V and +0.25 V. Corrosion current density C_{cd} (A/cm^2) and corrosion potential C_p (V) were calculated from the Tafel extrapolation method. Corrosion rate C_r (mm/y) was determined from the relationship below;

$$\mathrm{Cr} = \frac{0.00327 \times C_{cd} \times E_{qw}}{D} \quad (1)$$

where E_{qw} is the equivalent weight (g) of MS, 0.00327 is a constant for corrosion rate calculation in mm/y and D is the density (g). The inhibition efficiency I_e (%) was determined from the corrosion rate values according to equation (Akinyemi et al., 2012);

$$I_e = \left[1 - \left(\frac{C_{r2}}{C_{r1}}\right)\right] * 100 \quad (2)$$

C_{r1} and C_{r2} are the corrosion rate without and with SASC compound in the acid solution.

Weight loss analysis was performed on MS steel coupons individually submerged in 200 mL of the H_2SO_4/SASC test solution for 240 h and weighed every 24 h to determine the weight loss, corrosion rate, surface coverage and inhibition efficiency according to the equations below;

$$\mathrm{CR} = \left[\frac{87.6\omega}{DAt}\right] \quad (3)$$

ω is the weight loss (g), D is the density (g/cm^3), A is the total exposed surface area of MS and 87.6 is a constant. t is the time (h). Inhibition efficiency values (I_e) were calculated from the formula below;

$$\eta = \left[\frac{\omega_1 - \omega_2}{\omega_1}\right] * 100 \quad (4)$$

ω_1 and ω_2 are the weight loss at specific SASC concentrations. Surface coverage (θ) values were calculated from equation (5):

$$\theta = \left[1 - \frac{\omega_2}{\omega_1}\right] \quad (5)$$

Optical mages of corroded and inhibited MS surface morphology from optical microscopy were analyzed after weight-loss analysis with Omax trinocular.

3. Result and discussion

3.1. Electrochemical studies

The corrosion polarization behavior of MS in 1M H_2SO_4 solution at 0%, 1%, 2%, 3%, 4%, 5% and 6% SASC oil extract is shown on the anodic-cathodic polarization plots in Fig. 1. Data obtained from the plots are presented in Table 2. The slope of the anodic and cathodic plots for MS at 0% SASC is much higher than the slopes of MS at other SASC concentrations due to the corrosive actions of SO_4^{2-} anions within the acid solution in the absence of SASC molecules. The SO_4^{2-} anions react with the MS surface resulting in the oxidation of the Fe substrate metal which passes into the electrolyte as positive metallic cations after losing their valence electrons. Oxidation of MS causes the formation of porous oxides on the carbon steel surface which continues to grow. Hydrogen evolution and oxygen reduction reaction also occurs to counterbalance the anodic dissolution reactions. Under this condition the corrosion rate of the steel is 29.44 mm/y which correspond to a corrosion current density of 2.54 × 103 A/cm^2. Addition of SASC oil extract from 1% to 6% concentration altered the electrochemical

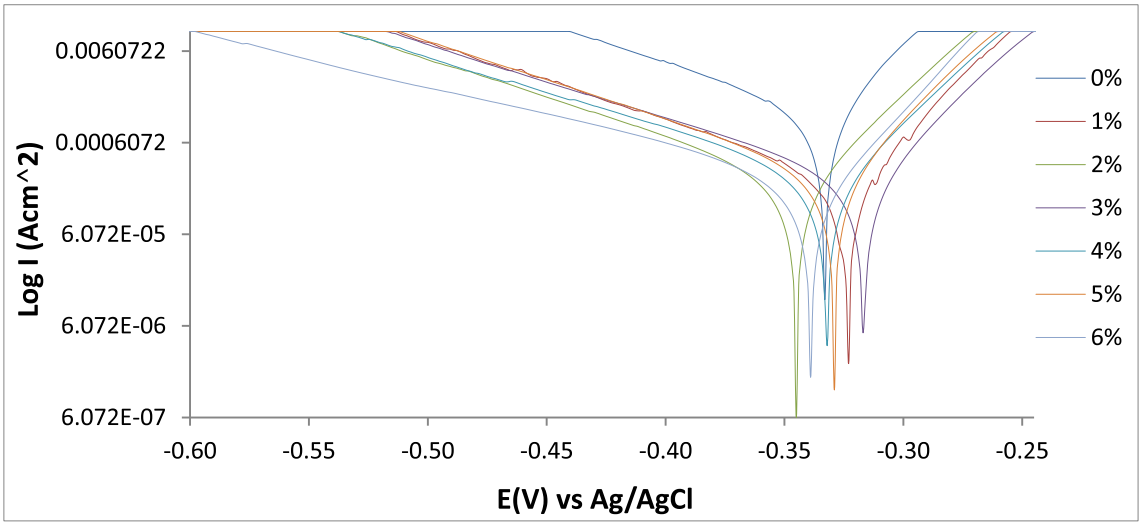

Fig. 1. Potentiodynamic polarization plots for MS corrosion in 1 M H_2SO_4 solution/0%–6% SASC concentration.

Table 2
Potentiodynamic polarization data for MS corrosion in 1 M H_2SO_4 solution/0%–6% SASC concentration.

Sample	SASC Conc. (%)	ROTC Conc. (M)	Corrosion Rate (mm/y)	SASC Inhibition Efficiency (%)	Corrosion Current (A)	Corrosion Current Density (A/cm^2)	Corrosion Potential (V)	Polarization Resistance, R_p (Ω)	Cathodic Tafel Slope, B_c (V/dec)	Anodic Tafel Slope B_a (V/dec)
A	0	0	29.44	0	2.63E-03	2.54E-03	−0.329	9.75	−8.027	1.233
B	1	4.52E-03	5.36	81.78	4.80E-04	4.62E-04	−0.319	53.52	−8.885	3.806
C	2	9.05E-03	4.73	83.95	4.23E-04	4.07E-04	−0.341	60.77	−8.457	9.883
D	3	1.36E-02	5.02	82.95	4.49E-04	4.33E-04	−0.313	57.75	−7.965	6.346
E	4	1.81E-02	4.76	83.85	4.26E-04	4.10E-04	−0.328	60.39	−7.783	9.438
F	5	2.26E-02	5.26	82.14	4.70E-04	4.53E-04	−0.325	56.35	−8.909	3.500
G	6	2.71E-02	3.95	86.58	3.54E-04	3.41E-04	−0.339	72.67	−6.662	6.450

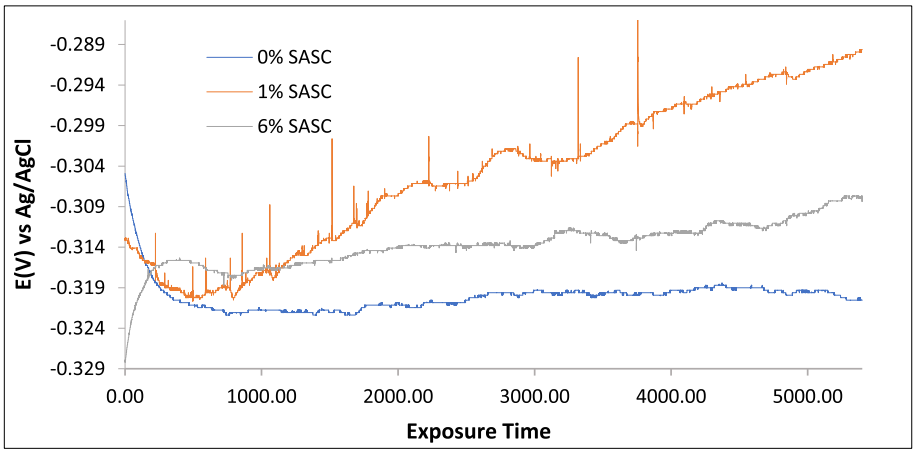

Fig. 2. Plot of open circuit corrosion potential ($V_{Ag/AgCl}$) versus exposure time (T) for 5400s.

Table 3
Data on weight loss, corrosion rate and inhibition efficiency from weight loss analysis at 240 h.

MS Samples	SASC Conc. (%)	SASC Conc. (M)	Weight Loss (g)	Corrosion Rate (mm/yr)	SASC Inhibition Efficiency (%)
A	0	0	6.234	48.05	0
B	1	0.0045	1.694	13.06	72.83
C	2	0.0090	1.410	10.87	77.38
D	3	0.0136	1.250	9.63	79.96
E	4	0.0181	1.218	9.39	80.46
F	5	0.0226	1.042	8.03	83.29
G	6	0.0271	1.291	9.95	79.29

process occurring on the steel surface. The corrosion rate declined sharply to 5.36 mm/y at 1% SASC coupled with significant change in polarization resistance from 9.75 Ω (0% SASC) to 53.52 Ω at 1% SASC. The transformation of the ionized metal surface from active dissolution state to state of surface protection is due to adsorption of SASC molecules onto the metal surface, forming a protective film (Chao et al., 1981). It must be noted that increase in SASC concentration has limited influence on the corrosion rate values, hence the inhibition efficiency values which peaked at 86.58 mm/y at 6% SASC from 81.78 mm/y at 1% SASC. The active-passive behavior of the corrosion potential values after 0% SASC shows SASC oil extract offers mixed type corrosion inhibition characteristics (Loto et al., 2014; Loto, 2017b). However, visible changes in anodic Tafel slope values compared to the cathodic counterpart show SASC has greater influence on the surface oxidation/anodic dissolution reactions. The cathodic Tafel slope values vary slightly depicting that the hydrogen evolution and oxygen reduction reactions are under activation control. This is further proven from the cathodic polarization plots from 2% to 5% SASC concentration. The marked differences in the slopes of the anodic plots align with the differences in anodic Tafel values indicating the inhibition mechanism of SASC is through surface coverage. Surface coverage reduces the availability of surface metal atoms for corrosion reactions thus suppressing the reaction mechanism (Lowmunkhong et al., 2010; Zhang et al., 2010; Hosseini and Azimi, 2009).

3.2. Open circuit potential measurement

The thermodynamic equilibrium properties of SASC inhibition on MS in 1M H_2SO_4 solution was studied at 0%, 1% and 6% SASC concentrations respectively. Fig. 2 shows the relationship between variation in corrosion potential with respect to exposure time for 5400s. At 0% SASC the corrosion potential of MS declined sharply to active values i.e. from −0.305 $V_{Ag/AgCl}$ (0s) to −0.322 $V_{Ag/AgCl}$ at 816.01s due to active corrosion reaction occurring on MS surface. The corrosion potential beyond this point remained generally stable with a final value of −0.321$V_{Ag/AgCl}$ at 5400s. At 1% SASC the corrosion potential of MS initiated at a more active value than 0% SASC probably due to delayed inhibition action of SASC molecules in the acid solution. This trend continued with the corrosion potential decreasing to −0.320 $V_{Ag/AgCl}$ at 584.10s, after which there is a progressive trend to the passive direction due to the inhibiting action of SASC till 5400 s at −0.290s. MS being a low carbon steel do not passivate in acid solutions because of the absence of chromium and other alloying elements that induces passivity. The oxide that forms on carbon steels are porous allowing corrosive anions to penetrate. This results in the continuous deterioration of the steel. However, in the presence of 1% SASC the visible transition of the OCP plot is due to the interference of electrochemical processes responsible for anodic dissolution by SASC molecules which undergoes certain degree of protonation in the acid solution. Based on the conclusions from the polarization studies, surface coverage is most likely the reason for the passivation behavior. Addition of 6% SASC induces higher electronegativity on the steel surface at the onset of the OCP test. The potential initiated −0.328 $V_{Ag/AgCl}$ (0s) and progressed to

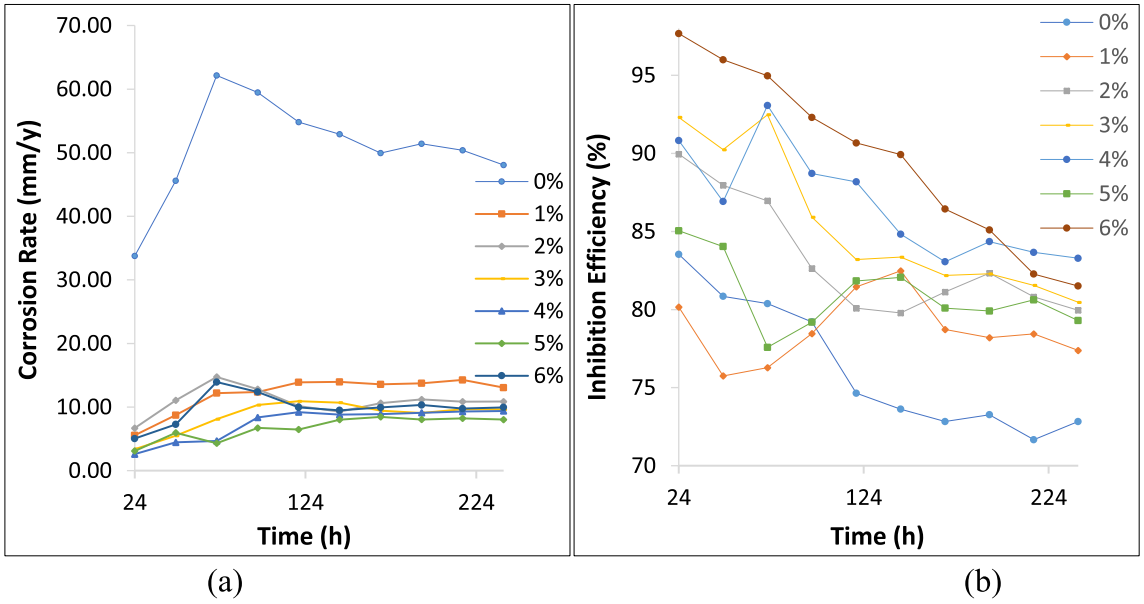

Fig. 3. Weight loss analysis plot of (a) corrosion rate versus exposure time, and (b) inhibition efficiency versus exposure time.

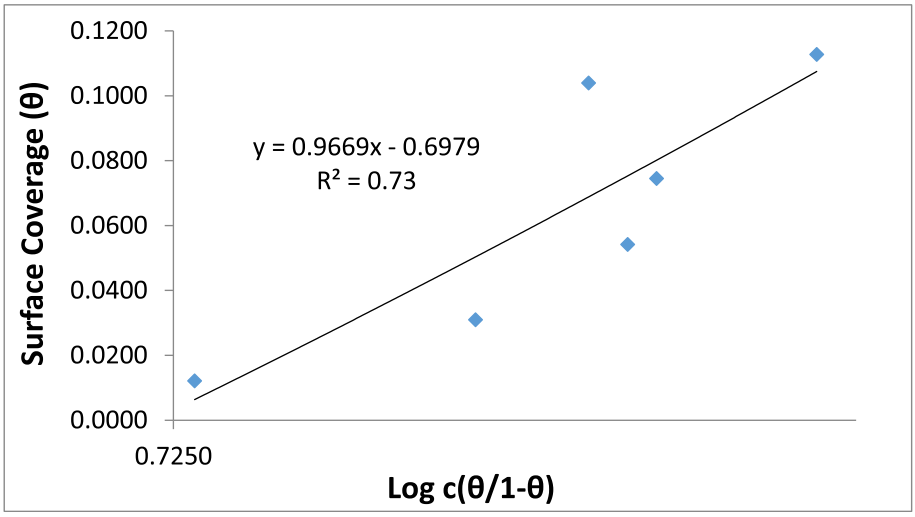

Fig. 4. Frumkin plot of SASC surface coverage (θ) vs log c [θ/1-θ].

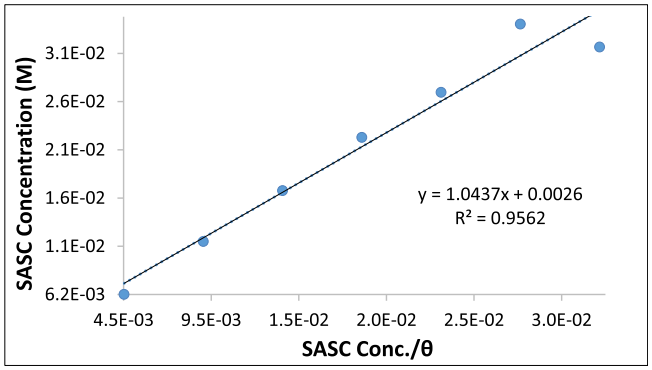

Fig. 5. Langmuir plot of SASC conc. versus SASC conc./θ.

relatively passive values at −0.316 $V_{Ag/AgCl}$ (424.7s). Beyond this value the thermodynamic behavior of MS at 6% SASC was relatively stable though a mild increase in potential occur peaking at −308 $V_{Ag/AgCl}$ (5400s).

3.3. Weight loss analysis

Data on weight loss and corrosion rate of MS, and inhibition of SASC compound at 0%–6% SASC concentration from weight loss analysis in 1 M H_2SO_4 solution after 240 h are shown in Table 3. Fig. 3(a) and (b) shows the plot of MS corrosion rate and SASC inhibition efficiency versus exposure time. In the absence of SASC inhibiting compound, MS corroded rapidly for the first 72 h attaining a corrosion rate value of 65.15 mm/y. Beyond this point a gradual decrease in corrosion rate was observed till 48.05 mm/y at 240 h. This behavior as earlier explained is due to anodic dissolution and interfacial deterioration of the surface properties of the steel. The behavior of MS strakly contrast the plots of MS upon addition of SASC to the acid media. The corrosion rate reduced sharply due to suppression of the electrochemical action of SO_4^{2-} by coverage of MS surface. As a result the reactive sites on the steel and blocked. SASC concentration plays a minor role on the inhibition efficiency values of SASC, thus the inhibiting action of SASC is concentration dependent.

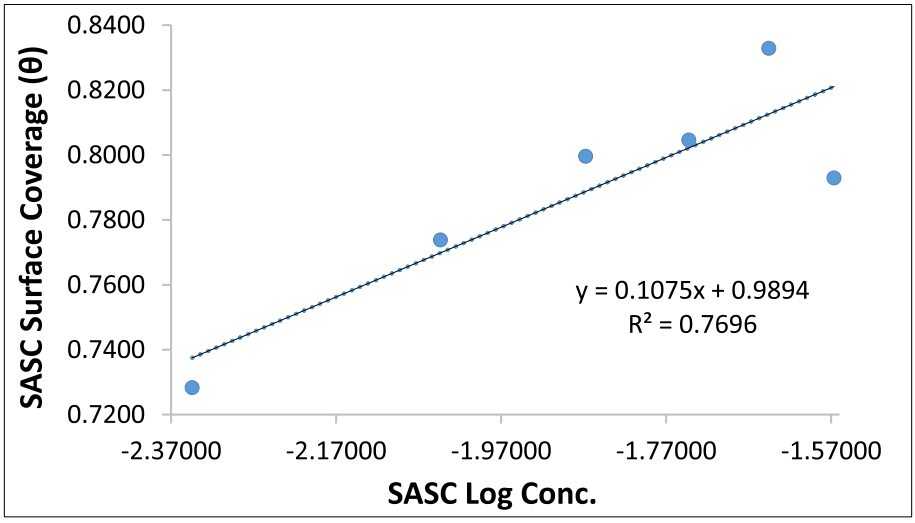

Fig. 6. Freundlich plot of SASC surface coverage versus SASC log conc.

Table 4
Calculated results of ΔG_{ads}, and K_{ads}.

MS Samples	SASC Conc. (%)	Surface Coverage (θ)	Equilibrium Constant of adsorption (K)	Gibbs Free Energy, ΔG ($Kjmol^{-1}$)
0	0	0	0	0
1	1	0.728	592539.2	−42.89
2	2	0.774	378096.4	−41.78
3	3	0.800	294002.0	−41.15
4	4	0.805	227557.9	−40.52
5	5	0.833	220365.1	−40.44
6	6	0.793	141053.4	−39.33

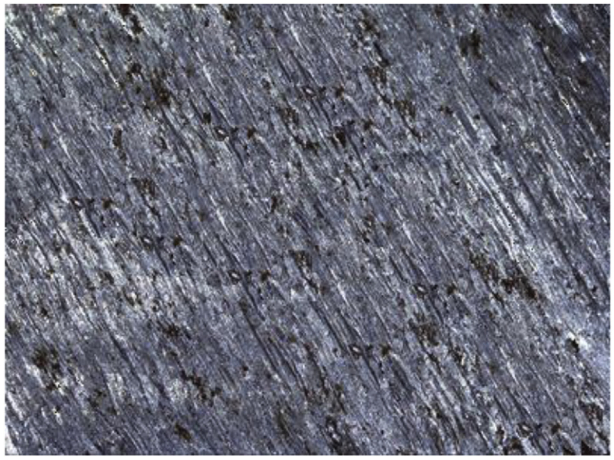

Fig. 7. Optical image of MS morphology before corrosion.

3.4. Adsorption isotherm and corrosion thermodynamics

Adsorption occurs during the corrosion inhibition process of SASC on MS in the acid media whereby SASC molecules accumulates at the metal solution interface. It is a surface phenomenon by which complex organic compounds is drawn to the surface of MS and adheres through physical chemical or electrostatic attraction. Adsorption isotherm models are used to explain adsorption data derived from experimental analysis. The models and the consequent thermodynamic derivations provide in depth information into the mechanism of adsorption mode of attraction and adsorption strength (Emrah et al., 2008; Porkodi and Kumar, 2007). Due to the admixture of H_2SO_4—H_2O molecules with the cationic molecules of SASC in the interfacial region the adsorption process is considered a replacement reaction of H_2SO_4—H_2O molecules with SASC molecules within the bulk solution (Gerente et al., 2007; Trasatti, 1974). The Frumkin, Langmuir and Freundlich isotherms shown in Figs. 4–6 provided the best fits among the isotherms tested with correlation coefficients of 0.7300, 0.9562 and 0.7696 respectively. According to Frumkin isotherm the surface coverage is subject to the potential of the steel surface due to variation in the energy of the double-layer capacitor. This results from the replacement of H_2O molecules water is replaced by the molecules of the organic derivatives with lower dielectric constant. The Frumkin equation is as follows;

$$\text{Log } [C_{SASC} * (\theta/_{1-\theta})] = 2.303 \log K_{ads} + 2a\theta \quad (6)$$

The Langmuir isotherm suggests the following with respect to the Langmuir equation below; (i) constant interfacial surface reaction, (ii) the extent of inhibitor coverage has no effect on Gibbs free energy values and (iii) the effect of lateral interaction resulting from the molecular reaction of adsorbates on the value of Gibbs free energy is negligible (Guidelli et al., 1992).

$$\theta = \left[\frac{K_{ads} C_{SASC}}{1 + K_{ads} C_{SASC}}\right] \quad (7)$$

The Freundlich isotherm delineates the association between adsorbed inhibitor molecules, their intermolecular reaction (repulsion or attraction) and effect on the mechanism of adsorption (Ashish and Quraishi, 2011). The Freundlich equation is as follows;

$$\theta = KC^{n} \quad (8)$$

$$\log \theta = n\log C + \log K_{ads} \quad (9)$$

n is a constant with respect to the characteristics of adsorbed MTH molecule, K_{ads} is the adsorption-desorption equilibrium constant representing the intermolecular strength of the adsorbed layer.

Adsorption of protonated molecules of the inhibiting compounds (SASC) occurs through covalent, physical or electrostatic attraction as earlier mentioned. However, to determine the nature and possibly the strength of SASC adsorption onto the steel surface, Gibbs free energy (ΔG_{ads}) was adopted to provide further insight to the thermodynamics of the corrosion process. The mathematical representation of ΔG_{ads} with respect to equilibrium constant of adsorption is shown in Table 4 below;

$$\Delta G_{ads} = -2.303RT \log [55.5K_{ads}] \quad (10)$$

55.5 is the molar concentration of water in the solution, R is the universal gas constant, T is the absolute temperature and K_{ads} is the

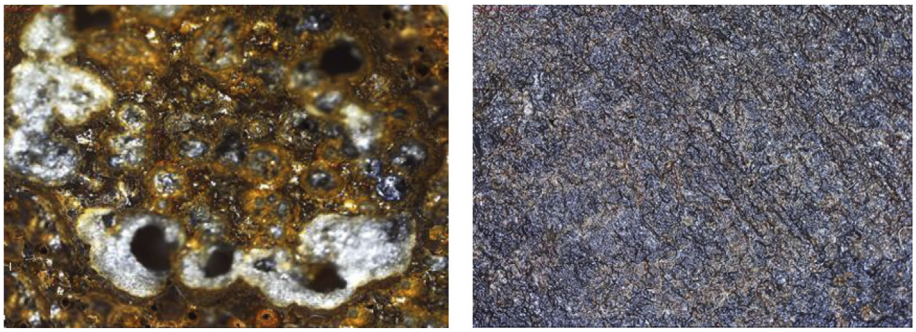

Fig. 8. Optical image of MS morphology (a) after corrosion in 0% SASC/1M H_2SO_4, and (b) after corrosion in 6% SASC/1M H_2SO_4.

equilibrium constant of adsorption of SASC molecules onto the steel. The equilibrium constant of adsorption was determined from the Langmuir adsorption isotherm due to its comparatively higher correlation coefficient value. ΔG_{ads} values depends on metallurgical variables such as micro-pits, non-metallic impurities, elemental arrangements, microscopic fissures and crevices with respect to grain orientation on the steel surface. Previous research has proven that ΔG_{ads} values around -20 kJ/mol or below depict physisorption adsorption characteristics (physical adsorption according to Vander waals forces), while values around -40 kJ/mol or above involve charge sharing or transfer (covalent or electrostatic attraction) between the SASC molecules and the steel surface due to chemisorption adsorption mechanism. The ΔG_{ads} values in Table 4 shows chemisorption adsorption mechanism. This enabled strong adsorption of SASC molecules resulting in effective blockage of reactive sites on the steels surface. The negative values of ΔG_{ads} show that SASC adsorption on MS is spontaneous. The decrease in ΔG_{ads} values with increase in SASC concentration is due to lateral repulsion among SASC molecules during the adsorption process (Solmaz, 2010; Döner et al., 2011; Loto et al., 2016).

3.5. Optical microscopic studies

Optical images of MS morphology before corrosion, and after corrosion test in 0% SASC/H_2SO_4 and 6% SASC/H_2SO_4 solution are shown from Fig. 7 to Fig. 8(b). The morphology of MS before corrosion (Fig. 7) shows lined and serrated edges due to machining and sample preparation. Surface oxide are few, very small and quite negligible. The morphology of MS in Fig. 8(a) is due to the electrochemical action of SO_4^{2-} resulting severe general surface deterioration, rust and corrosion pits. The SO_4^{2-} anions penetrates through the surface oxide due to its porosity accelerating the electrochemical reactions afterwards which destroys the metal substrate. The electrochemical reaction involves charge transfer between the anodic and cathodic reactions on the steel in the acid solution. The limited alloy content of carbon steel does not generally produce any remarkable changes in its general corrosion resistance. In 6% SASC/H_2SO_4 solution, a remarkable change in MS morphology is clearly visible due to the inhibiting action of SASC. Previous discussion from electrochemical tests and adsorption studies shows SASC molecules adheres to MS surface through chemisorption mechanism whereby the inhibitor forms an impenetrable protective film on the steel. The limited surface deterioration in comparison to the morphology in Fig. 7 is probably due to preabsorbed SO_4^{2-} anions which ionizes the surface of the steel and furthermore favors electrostatic attraction of SASC molecules.

4. Conclusion

The synergistic combination of salvia officinalis and simmondsia chinensis effectively inhibited the corrosion of mild steel in dilute H_2SO_4 solution with inhibition efficiency values generally above 80%. The organic derivatives formed a protective film on the steel as shown on the inhibiting micro-analytical image, inhibiting the electrochemical action of the corrosive species through chemisorption mechanism. The inhibition performance of compound was observed to be concentration dependent with mixed inhibition properties though Tafel slope values showed higher tendency for anodic inhibition.

Conflict of interest

The authors declares no conflict of interest for the manuscript submitted.

Acknowledgement

The author recognizes the support given by Covenant University Ota, Ogun State, Nigeria towards the sponsorship, implementation and successful completion of the research.

Appendix A. Supplementary data

Supplementary data related to this article can be found at https://doi.org/10.1016/j.sajce.2018.09.002.

References

Akinyemi, O.O., Nwaokocha, C.N., Adesanya, A.O., 2012. Evaluation of corrosion cost of crude oil processing industry. J. Eng. Sci. Technol. 7 (4), 517–528.
Ashish, K.S., Quraishi, M.A., 2011. Investigation of the effect of disulfiram on corrosion of mild steel in hydrochloric acid solution. Corrosion Sci. 53 (4), 1288–1297.
Camila, G.D., Alexandre, F.G., 2013. Corrosion inhibitors – principles, mechanisms and applications, Developments in corrosion protection. Intechopen 365–379. https://doi.org/10.5772/57255.
Chao, C.Y., Lin, L.F., Macdonald, D.D., 1981. Point defect model for anodic passive films. J. Electrochem. Soc. 128, 1187–1194.
Cicek, Volkan, 2017. Chromates: Best Corrosion Inhibitors to Date, Corrosion Engineering and Cathodic Protection Handbook. Scrivener Publishing LLC, Inc, pp. 27–30. https://doi.org/10.1002/9781119284338.ch11.
Corrosion Costs and Preventive Strategies in the United States, NACE Publication NO. FHWA-RD-01-156. https://www.nace.org/uploadedFiles/Publications/ccsupp.pdf. (accessed 08:06:2018).
Dakeshwar, K.V., Fahmida, K., 2015. Corrosion inhibition of mild steel by extract of bryophyllum pinnatum leaves in acidic solution. Chem. Mater. Res. 7 2225-0956.
David, A.W., 2017. Predicting the performance of organic corrosion inhibitors. Metals 7 (12), 553. https://doi.org/10.3390/met7120553.
Deepak, D., Kateřina, L., Thomas, B., 2017. Carbon steel corrosion: a review of key surface properties and characterization methods. RSC Adv. 8, 4580–4610.
Döner, A., Solmaz, R., Özcan, M., Kardaş, G., 2011. Experimental and theoretical studies of thiazoles as corrosion inhibitors for mild steel in sulphuric acid solution. Corrosion Sci. 53 (9), 2902–2913.
Emrah, B., Mahmut, O., Sengil, I.A., 2008. Adsorption of malachite green onto bentonite: equilibrium and kinetic studies and process design. Microporous Mesoporous Mater. 115, 234–246.
Essential oil. https://en.wikipedia.org/wiki/Essential_oil. (accessed 08:06:2018).
Fouda, A.S., Diab, M.A., Fathy, S., 2017. Role of some organic compounds as corrosion inhibitors for 316L stainless steel in 1 M HCl. Int. J. Electrochem. Sci. 12, 347–362.
Gerente, C., Lee, V.K.C., Le Cloırec, P., McKay, G., 2007. Application of chitosan for the removal of metals from wastewaters by adsorption—mechanisms and models review. Crit. Rev. Environ. Sci. Technol. 37 (1), 41–127.

Guidelli, R., 1992. In: Kowski, J.L., Ross, P.N. (Eds.), Adsorption of Molecules at Metal Electrodes. VCH Publishers, lnc., New York, pp. 1.
Hosseini, S.M.A., Azimi, A., 2009. The inhibition of mild steel corrosion in acidic medium by 1-methyl-3-pyridin-2-yl-thiourea. Corrosion Sci. 51, 728–732.
Jekayinfa, S.O., Okekunle, P.O., Amole, P.I.G., Oyelade, J.A., 2015. Evaluation of corrosion cost in some selected food and agro-processing industries in Nigeria. Anti. Corros. Method. M. 52 (4), 214–218.
K. Elaya, P.K., 2014. Corrosion risk analysis, risk-based inspection and a case study concerning a condensate pipeline. Procedia Eng 86, 597–605.
Kuznetsov, Y.I., 1996. Organic Inhibitors of Corrosion of Metals. Springer UShttps://doi.org/10.1007/978-1-4899-1956-4.
Loto, R.T., 2017a. Corrosion inhibition effect of non-toxic α-amino acid compound on high carbon steel in low molar concentration of hydrochloric acid. J. Mater. Res. Technol. https://doi.org/10.1016/j.jmrt.2017.09.005.
Loto, R.T., 2017b. Comparative analysis of the synergistic effect of sodium molybdenum oxide and vanillin on the corrosion inhibition of 3CR12 ferritic stainless steel and high carbon steel in dilute hydrochloric acid. J. Bio. Tribo. Corros. 3 (17). https://doi.org/10.1007/s40735-017-0077-0.
Loto, R.T., Loto, C.A., T.I, 2013. Electrochemical studies of mild steel corrosioninhibition in sulfuric acid chloride by aniline. Res. Chem. Intermed. 40 (4), 1501–1516.
Loto, R.T., Loto, C.A., Popoola, A.P.I., 2014. Electrochemical Studies of the corrosion inhibition effect of 2-amino-5-ethyl-1, 3, 4-thiadiazole in on low carbon steel in dilute sulphuric acid. J. Chem. Soc. Pakistan 36 (6), 1043–1051.
Loto, R.T., Loto, C.A., Joseph, O.O., Gabriel, O., 2016. Adsorption and corrosion inhibition properties of thiocarbanilide on the electrochemical behavior of high carbon steel in dilute acid solutions. Result in Physics 6, 305–314.
Loto, R.T., Loto, C.A., Ayozie, B., Sanni, T., 2018. Anti-corrosion properties of rosemary oil and vanillin on low carbon steel in dilute acid solutions. In: The Minerals, Metals & Materials Society, TMS 2018 147th Annual Meeting & Exhibition Supplemental Proceedings, the Minerals. Metals & Materials Series, pp. 883–890. https://doi.org/10.1007/978-3-319-72526-0_84.
Lowmunkhong, P., Ungthararak, D., Sutthivaiyakit, P., 2010. Tryptamine as a corrosion inhibitor of mild steel in hydrochloric acid solution. Corrosion Sci. 1 (52), 30–36.
Obot, I.B., Obi-Egbedi, N.O., Umoren, S.A., Ebenso, E.E., 2010. Synergistic and antagonistic effects of anions and ipomoea invulcrata as green corrosion inhibitor for aluminium dissolution in acidic medium. Int. J. of Electrochem. Sci. 5 (7), 994–1007.
Porkodi, K., Kumar, K.V., 2007. Equilibrium, kinetics and mechanism modeling and simulation of basic and acid dyes sorption onto jute fiber carbon: eosin yellow, malachite green and crystal violet single component systems. J. Hazard Mater. 143, 311–327 (2007).
Rivera-Grau, L.N., Casales, M., Regla, I., Ortega-Toledo, D.M., Ascencio-Gutierrez, J.A., Porcayo-Calderon, J., Martinez-Gomez, L., 2013. Effect of organic corrosion inhibitors on the corrosion performance of 1018 carbon steel in 3% NaCl solution. Int. J. Electrochem. Sci. 8, 2491–2503.
Sanyal, B., 1981. Organic compounds as corrosion inhibitors in different environments — a review. Prog. Org. Coating 9 (2), 165–236.
Singh, W.P., Bockris, J.O., 1996. Toxicity Issues of Organic Corrosion Inhibitors: Applications of QSAR Model. NACE International.
Solmaz, R., 2010. Investigation of the inhibition effect of 5-(E)-4-phenylbuta-1,3-dienylideneamino)-1,3,4-thiadiazole-2-thiol Schiff base on mild steel corrosion in HCl acid. Corrosion Sci. 52 (10), 3321–3330.
Subhashini, S., Rajalakshmi, R., Prithiba, Mathina, A., 2010. Corrosion mitigating effect of cyamopsis tetragonaloba seed extract on mild steel in acid medium. E-J. of Chem. 7 (4), 1133–1137.
The Effects and Economic Impact of Corrosion, Corrosion: Understanding the Basics. ASM International. www.asminternational.org/documents/10192/1849770/06691g_chapter_1.pdf, Accessed date: 8 June 2018.
Trasatti, S., 1974. Acquisition and analysis of fundamental parameters in the adsorption of organic substances at electrodes. J. Electroanal. Chem. 53 (3), 335–363.
Winkler, D.A., Breedon, M.A., Hughes, E., Burden, F.R., Barnard, A.S., Harvey, T.G., Cole, I., 2014. Towards chromate-free corrosion inhibitors: structure–property models for organic alternatives. Green Chem. 16, 3349–3357.
Zhang, S., Tao, Z., Li, W., Hou, B., 2010. Substitutional adsorption isotherms and corrosion inhibitive properties of some oxadiazol- triazole derivative in acidic solution. Corrosion Sci. 9 (52), 3126–3132.